IEEE Robotics and Automation Letters (RA-L) paper, presented at ICRA 2024, Yokohama, Japan. Cite as RA-L paper.

Feedforward Control of Lower Limb Exoskeletons: which torque profile should we use?

Hannah Dinovitzer[1], Mohammad Shushtari[1] *Student Member*, *IEEE*, and Arash Arami[1,2*] *Member*, *IEEE*

***Abstract*—Despite the increased use of lower limb exoskeletons as gait training and mobility assistive devices, their controllers often lack the ability to synchronize and adapt to meet individual users' needs. This paper investigates two control approaches for lower limb exoskeletons: a real-time kinematic state-dependent estimation of desired torques with an inverse dynamics model and a data-driven component in the first approach, and a pre-defined torque control based on gait speed and phase in the second approach. These controllers are linearly combined to shift the controller behavior between pure kinematic state-dependent and pure gait phase-dependent control. These combinations were tested during overground and treadmill walking with nine able-bodied participants. The linearly combined controller with a greater emphasis on kinematic state-dependent control produced a more natural gait in terms of spatiotemporal metrics. This is reflected by 0.1m/s increases in overground walking speed and 5% decrease in percent stance compared to walking with a passive exoskeleton. This controller also decreases the overall activity of lower limb muscles by up to 25% and thigh co-contractions by up to 40%. Participant feedback through a questionnaire, in terms of perceived effort, walking naturalness, and stability, also favored the aforementioned controller.**

***Index Terms*—Gait, dynamic modelling, exoskeleton control, data-driven modelling, rehabilitation**

I. Introduction

ASSISTIVE and rehabilitation exoskeletons have shown promise in enabling individuals with lower limb motor deficits to walk again. Despite advances in exoskeleton design [1] the controller design for effective human-exoskeleton interaction is still a challenge [2]. Enhancement in the control methods is expected to greatly improve the overall performance of assistive exoskeletons [2]. Particularly, in partial assistive control, where the exoskeleton provides assistance-as-needed (AAN) and the user also contributes to movements, challenges arise due to problems with human-robot coordination and synchronization. There are many approaches to implement AAN control, including path control [3], flow control [4], virtual energy regulation [5], trajectory adaptation [6], and neuromechanical model-based control [7].

In some studies, joint trajectories were predicted using a dual unscented Kalman filter [8] or adapted using interaction torque [6] and used alongside an impedance controller that applies torque at the joint to maintain the user's joint angles about these perceived desired trajectories, assuming accurate estimation of user's intended trajectories. However, the effectiveness of this approach for individuals with motor deficits is uncertain and needs more investigations [6].

Alternatively, feedforward torque controllers have been used in assistive robotic scenarios, for instance, to make wearable robotic systems transparent [9], i.e., compensating for the dynamics of the robot. The user required joint torques can be estimated and used as the desired exoskeleton joint torques [10], [11] to develop a synchronized AAN control. There have been various dynamics-based approaches to estimating joint torques. Some approaches apply only certain components of the joint torques while others use simplified or detailed models of the human lower body to estimate and apply all components of joint torques. A control strategy constructed in the torque domain is advantageous as it does not explicitly enforce any joint trajectories [12].

A simple approach for joint torque computation is to generate a set of pre-defined torques based on gait phase and/or walking speed [13]. This approach involves using the averaged required torques across participants or walking conditions, rather than tailoring the torque to each individual user. However, pre-defined torque profiles can be restrictive to the user and hinder natural variations in walking dynamics.

In quasi-static movements, some approaches consider only gravitational effects and effects of the ground reaction forces (GRFs) mapping as they dominate exoskeleton dynamics. For instance, a gravity compensation control strategy reduced the participant's energy expenditure during periodic squatting [14-16]. As this approach is intended for quasi-static movements, it is not intended for use while walking.

In [10], a gravity compensator with GRF information is used to provide assistive torques during walking. Although in these studies gravity and force mapping compensation is shown to assist, this approach is not ideal for dynamic movements, e.g., walking, as inertial forces (due to the resistance of distributed mass across segments with changing velocities) and Coriolis forces (due to a multi-joint system with non-zero joint velocities) have greater roles, compensating their effect can thus provide a more desirable assistance.

Simplified models, such as a spring-loaded inverted pen-

Manuscript received: May 16, 2023; Revised: August 28, 2023; Accepted: October 14, 2023. This paper was recommended for publication by Editor Jee-Hwan Ryu upon evaluation of the Associate Editor and Reviewers' comments. This work was supported by NSERC Discovery Grant RGPIN-2018-04850, the John R. Evans Leaders Fund Canadian Foundation for Innovation, Ontario Research Fund (ORF), and New Frontiers in Research Fund - Exploration NFRFE2018-01698.

[1] Hannah Dinovitzer, Mohammad Shushtari, and Arash Arami are with the Department of Mechanical and Mechatronics Engineering, University of Waterloo, Waterloo, ON N2L 3G1, Canada hdinovitzer@uwaterloo.ca; smshushtari@uwaterloo.ca; arash.arami@uwaterloo.ca.

[2] Arash Arami is also with Toronto Rehabilitation Institute (KITE), University Health Network, Toronto, ON M5G 2A2, Canada.

* *Corresponding author: Arash Arami.*

Digital Object Identifier (DOI): see top of this page.

IEEE Robotics and Automation Letters (RA-L) paper, presented at ICRA 2024, Yokohama, Japan. Cite as RA-L paper.

IEEE Robotics and Automation Letters (RA-L) paper, presented at ICRA 2024, Yokohama, Japan. Cite as RA-L paper.

dulum model (SLIP) [17], are implemented to estimate the required joint torques. This approach was only implemented during stance phase, leaving the swing phase unassisted. A compass-gait model is implemented [18], in which the swing leg is simplified to a 2 degree-of-freedom (DoF) manipulator and is controlled across a periodic limit cycle. Both these controllers can only be implemented for portions of the gait cycle rather than across the entirety of the gait cycle.

In [19], the whole dynamics, including gravity, inertia, and Coriolis effects are considered in estimating the joint torques. The gait cycle is split into four sections, each having separate dynamical equations describing the joint torques. As the joint torque estimation switches between four models, there are discontinuities in the estimation, which renders this approach undesirable for implementation as an exoskeleton controller. To solve this, all components in the Lagrangian equation is taken into account leading to a single dynamical equation that describes the joint torques in all of the gait phases [11]. In this case, the foot contact forces and center of pressure (COP) are measured using instrumented insoles and then considered in the torque computations. The use of instrumented insoles can be challenging in terms of accuracy and real-time processing.

To address the shortcomings of the previously discussed approaches, [20] recently proposed an accurate and real-time approach to joint torque estimation that can be implemented in any setting, including those without force measurements. Having an accurate method of joint torque estimation which requires only kinematic measurements will facilitate biomechanical analysis in settings where force measurement is challenging such as continuous overground walking.

In this paper, for the first time, this real-time joint torque estimator is used as a controller to apply torque to the exoskeleton joints. Investigations are done to compare the performance of this controller with a pre-defined torque controller when used by able-bodied participants.

II. Methods and Material

A. Control strategies

Two main torque control strategies are implemented: Gait-phase dependent and Kinematic state-dependent torque control. In addition, linear combinations of these two controllers are tested with different weights resulting in 4 controllers being investigated and compared.

1) Gait phase-dependent torque control (GPC): In the gait phase-dependent torque controller (GPC) the gait phase was first estimated using [21] and the gait speed was computed by step length (computed using forward kinematics) divided by the step time. The torque profile was then determined according to gait phase using a lookup table.

The look-up table was generated from measured exoskeleton joint torques obtained from the interaction with one participant. Torques are the result of a high-gain proportional-derivative (PD) controller when the participant was walking with the exoskeleton and the reference trajectories were obtained from the participant's walking without the exoskeleton. The proportional (K_p) and derivative (K_d) gains at the hip were 3 and 0.25, respectively. At the knee, these gains were 0.9 and 0.08, respectively. Joint torques were measured at a series of speeds ranging from 0.4 to 1.2 m/s, then normalized by the subject's body weight$\times$height, then resampled to form a lookup table based on the estimated gait phase and speed.

The torques are not fully personalized for each individual as this controller was intentionally designed based on data from a single participant. This approach was driven by the aim of this study to also assess the feasibility of torque controllers that can be tested in future works on individuals with motor impairments, where measuring personalized torque profiles is impractical. Using the similarities in joint torque profiles between individuals during gait, demonstrated in previous studies [22], the joint torque profile for each individual was normalized by their body mass and height.

2) Kinematic state-dependent torque control (KSC): The joint torque estimator presented in [20] was modified to be used in real-time with exoskeleton-measured signals, now referred to as the Kinematic State-Dependent Torque Control (KSC). The torque estimator consists of an inverse dynamic model and a neural network (ANN) for GRF and Zero Moment Point (ZMP) estimation (Fig.2A). At ZMP the reaction and applied forces cancel and generate no moment about this point. The overall dynamic equation is as follows,

$$\hat{\tau} = H \begin{bmatrix} \ddot{p}_0 \\ \ddot{q}_0 \\ \ddot{q} \end{bmatrix} + B - K_R \begin{bmatrix} \hat{F} \\ \hat{N} \end{bmatrix}_R - K_L \begin{bmatrix} \hat{F} \\ \hat{N} \end{bmatrix}_L \quad (1)$$

where H is the inertia matrix, $p_{i,0}$ and $q_{i,0}$ are the position and orientation of the base link (pelvis) in relation to the global coordinate system, q and τ are vectors of six joint angles and torques respectively, K_R and K_L are the matrices that map the ground reaction forces and torques to base coordinates, B is the Coriolis and gravitational forces acting on the body segments, and $\hat{F}$ and $\hat{N}$ are vectors of estimated ground reaction forces and torques on the left (L) and right (R) foot. In order to determine the global position and orientation of the exoskeleton, p_0 and q_0, the inertial measurement units (IMUs) in the exoskeleton were used along with rigid body kinematic equations. Moreover, the K_R and K_L matrices are determined using the linear position of the ankle joint with respect to global coordinates, which is computed using feed forward kinematics. As the exoskeleton being used does not measure ankle kinematics, the ANN for GRF and ZMP estimation was trained to require only knee and hip kinematics on the same dataset used in [20].

The ANN contains two hidden layers of 20 and 10 neurons and was trained using the Levenberg-Marquardt algorithm [23] to minimize a mean squared error loss computed on GRF and ZMP measurements, respectively. The anterior-posterior component of ZMP has been utilized as the position for force application to the base link to eliminates the need for considering ground reaction moments in the force mapping.

3) Linear combination of controllers: The KSC and the GPC controllers were then linearly combined with the weight of w and $1 - w$, respectively. In addition to the pure KSC ($w = 1$) and GPC ($w = 0$) methods, two different linear

IEEE Robotics and Automation Letters (RA-L) paper, presented at ICRA 2024, Yokohama, Japan. Cite as RA-L paper.

IEEE Robotics and Automation Letters (RA-L) paper, presented at ICRA 2024, Yokohama, Japan. Cite as RA-L paper.

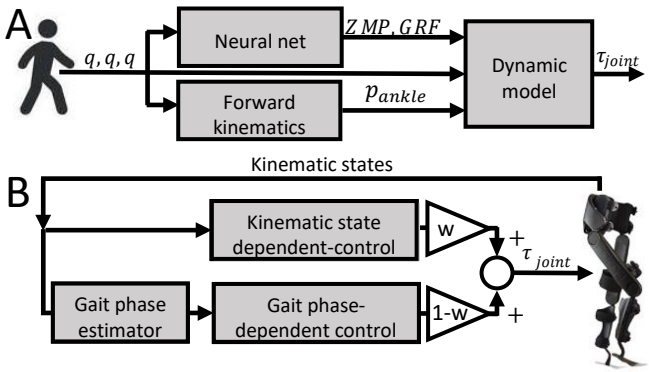

Figure 1. (**A**) Kinematic State-Dependent Torque Controller (KSC) block diagram based on the torque estimator in [20]. Ankle joint position (p_{ankle}) is computed using forward kinematics. The ZMP and GRF are estimated using an ANN. These information are then fed into the human dynamical model to obtain the human required joint torques. (B) Linear combination of the KSC and the gait phase-dependent torque controllers (GPC). Adjusting w gain, control strategy can shift linearly from KSC to GPC.

combinations were also tested with w = 0.75, including 75% KSC with 25% GPC, and w = 0.25, including 25% KSC with 75% GPC. These two combined controllers will be referred to as: 1G-3K, and 3G-1K, respectively.

B. Experimental setup

The experimental setup consists of a split-belt instrumented treadmill (Bertec, US), a lower limb exoskeleton (Indego, Parker Hannifin, US), six IMUs (MTw Awinda, Xsens, NL), and 12 electromyography (EMG) sensors (Trigno, Delsys, US). The exoskeleton, IMUs, and EMGs have sampling rates of 200, 100, and 2000 Hz, respectively. The EMG sensors were placed on both legs on the following muscles: rectus femoris (RF), vastus medialis (VM), bicep femoris (BF), tibialis anterior (TA), gastrocnemius medialis (GM), and soleus (SO). The IMUs were placed on each forefoot, the lateral aspect of shank, right thigh and torso. Fig. 2 shows the exoskeleton and sensor placements. The exoskeleton has actuated hip and knee joints with no actuation at the ankles.

Nine able-bodied participants (age 26±3.0 years, 7 male, mass: 74.6±8.8 kg, height: 182±6.5 cm) participated. Data collection protocols and procedures were approved by the Clinical Research Ethics Committee at the University of Waterloo (ORE#41794), and conformed with the Declaration of Helsinki. The experiment included both overground and treadmill walking during six different conditions. The conditions include one with passive exoskeleton, four with active exoskeleton (one for each controller), and one natural walking trial without the exoskeleton. The passive exoskeleton case is when the exoskeleton applies no torques to the joints while during the active cases, the exoskeleton applies the torques commanded by the controllers to each joint.

The participants walked on the treadmill at 0.6 and 0.8m/s for 40 seconds each. The participant then walked overground for a total of 36m at a self-selected walking pace for each of the six conditions. A questionnaire was completed immediately following each walking trial, at the same time the participants were given a one-minute resting period.

Figure 2. Lower limb exoskeleton and placement of EMG and IMU sensors.

Each participant, without being informed about the type of controller, was asked to rank the exoskeleton trials from 1 to 5 where 1 is the best in the following categories: effort level, stability, natural walking, and overall performance. Each category definition was intentionally left up to the interpretation of the participant to prevent bias and ensure responses considered individual priorities.

C. Data analysis

The IMU and EMG data are processed to compute various performance metrics. IMU signals are used for gait event detection and ankle joint angle calculation, while EMG data is processed to quantify muscle activity.

1) Gait event detection: The shank gyroscope measurements are used for heel strike and toe-off detection as done in [24], respectively. The detected heel strike and toe-off are used to determine stance and step duration. Using the detected heel strike events, all measured data is then segmented into gait cycles for further analysis.

2) Kinematic and spatiotemporal computations: IMUs are used to compute the ankle joint angles similar to [25] as the ankle joint angles are not measured by the exoskeleton's motor encoders. A principal component analysis (PCA) is applied to the gyroscope data of each IMU during the functional calibration movements [26].

As walking with heavy loads, like a backpack or heavy exoskeleton, can substantially alter joint-level kinematics [27], [28], it is expected to see significant changes between the exoskeleton conditions compared to natural walking. A controller that is able to effectively assist the user should render kinematics more similar to natural walking than passive exoskeleton walking. To evaluate this, the range of motion (ROM) of each joint is computed for each stride, along with the average Pearson correlation coefficient between the joint kinematics of natural and exoskeleton walking for each participant. Additionally, step lengths are computed from the foot IMU data similar to [29].

3) EMG processing: The EMG data was bandpass filtered, with cutoff frequencies of 5 and 100 Hz. The signal was then full-wave rectified and its envelope was computed by taking the moving average with a window of 50 ms. Each EMG signal is normalized by its respective maximum voluntary

IEEE Robotics and Automation Letters (RA-L) paper, presented at ICRA 2024, Yokohama, Japan. Cite as RA-L paper.

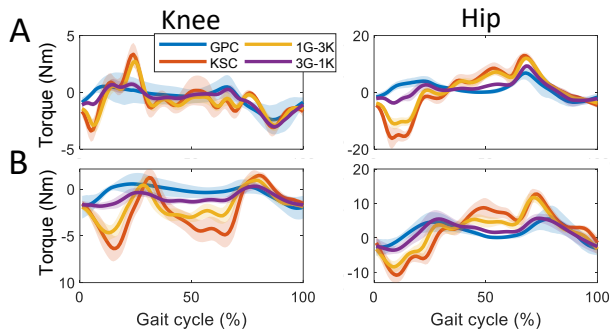

Figure 3. Average command torque for (A) participant 2, and (B) participant 6 for each controller while treadmill walking at 0.8m/s. The shaded area shows the standard deviation of the torques.

contraction (MVC), computed for each muscle as the maximum measured contraction during exoskeleton walking.

Based on the EMG activation during each stride, a measure of effort is computed as the integral of the squared EMG activation [30]. For the overground walking trials, as the walking speed is not fixed between trials or participants, the EMG measurements are normalized by walking speed. Additionally, the co-contraction between agonist-antagonist muscle pairs was compared across conditions. These pairs are RF-BF, VM-BF, TA-GM, and TA-SO. The co-contraction is computed using the product of the two muscle activation signals [31]. Similar to muscle effort, the co-contraction in each stride is quantified by the integral of the co-contraction signal during each step and is normalized by walking speed.

4) Statistical analysis: The first five steps of each condition were excluded to eliminate the transition effects of speed changes and adjustments to different controllers. Each metric was computed for each controller and each participant separately at each gait condition and then averaged across all gait cycles of that condition. The statistical differences of each metric across controllers were tested with a one-tailed Wilcoxon signed rank test. For spatiotemporal and kinematic metrics, a Bonferroni correction was applied [32]. Walking speed, step time, step length, and stance percentage were analyzed. Step width and lateral sway were not considered as the exoskeleton restricts movement to the sagittal plane in the knee and hip joints. As this exoskeleton does not control the ankle joint, spatiotemporal metrics which are primarily affected by the ankle angle, such as strike foot angle, and lift-off foot angle, were not considered. The spatiotemporal metrics were computed for each subject and compared to their respective metrics during natural walking.

III. Results and Discussion

As the controllers have only been tested on able-bodied participants, their potential for use for individuals with motor deficits remains unexplored. Yet, this study's findings lay the groundwork for future work involving individuals with incomplete spinal cord injuries.

A. Applied torques

The applied torques are plotted in Fig. 3 for two randomly selected participants walking on the treadmill at 0.8 m/s.Compared to GPC, KSC demonstrates a more personalized control torque specific to each participant, however, with higher variability. Their linear combination presents a trade-off between the two, depending on the combination weights.

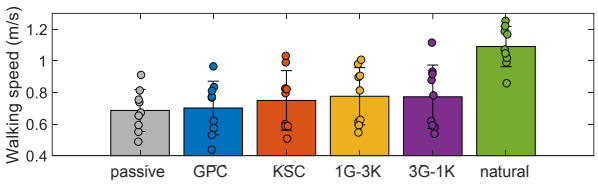

Figure 4. Overground walking speed of exoskeleton with different controllers and natural walking speed without the exoskeleton. The points show each participant's mean speed and the error bars show the standard deviation.

B. Spatiotemporal gait analysis

Fig. 4 shows the average overground walking speed. The 1G-3K has the fastest and closest speed to natural walking without the exoskeleton. The 3G-1K exhibits a slightly lower speed. The 1G-3K and 3G-1K controllers result in significantly faster walking than KSC and GPC ($p<0.004$).

The average standard deviation of walking speed without the exoskeleton for overground and treadmill walking is 0.059 and 0.035m/s, respectively. During overground walking, the 1G-3K has the most similar to natural walking speed variation equal to 0.062m/s. A higher walking speed can indicate the effectiveness of an assistive controller, while a greater natural variation in speed suggests a more natural gait and increased comfort of the participants with the controller overall. These results suggest that 1G-3K offers effective assistance while maintaining stability for overground walking.

Fig. 5 shows the percent change in percent stance, step time, and step length for each exoskeleton trial from natural walking of each respective subject. Overall, 1G-3K has a performance closest to natural walking in terms of spatiotemporal metrics. During treadmill walking at 0.6m/s, the passive case has a percent stance significantly ($p<0.002$) closer to natural walking compared to GPC. There are no significant differences for the other conditions and speeds ($p>0.0098$).

Studies have shown that an increase in percent stance time indicates decreased stability [33]. On average, GPC has the highest percent stance during overground walking, in agreement with participant feedback (see section III-F), demonstrating GPC is least favorable in terms of stability. During treadmill walking, the percent stance of the controllers are similar; however, the participant feedback also indicates that GPC is on average perceived as the least stable.

During overground walking, the 1G-3K has the percent stance most similar to natural walking. The performance of 1G-3K is closely followed by the KSC, with no significant differences between the different controllers during overground walking ($p>0.0195$). In treadmill trials, the passive condition has the closest percent stance to the natural gait, followed by KSC. Only the passive condition is significantly ($p<0.002$) closer to natural walking, while the other conditions show no significant difference. Overall, the 1G-3K and KSC showed the closest percent stance for overground and treadmill walking, respectively.

IEEE Robotics and Automation Letters (RA-L) paper, presented at ICRA 2024, Yokohama, Japan. Cite as RA-L paper.

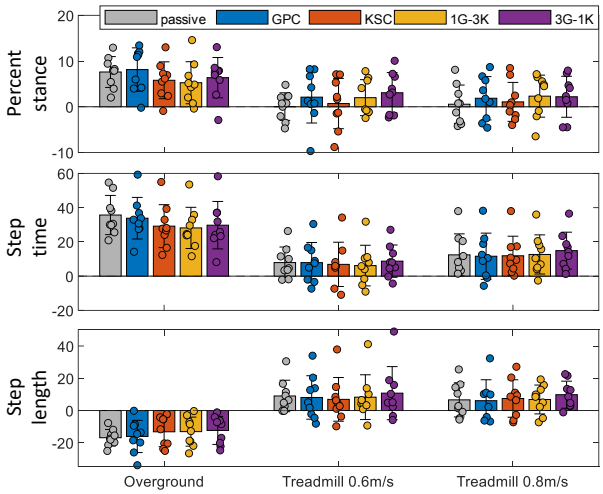

Figure 5. Spatiotemporal analysis of overground and treadmill walking at 0.6 and 0.8 m/s. Average difference of (A) percent stance, (B) step time, and (C) step length with respect to the natural walking at each condition.

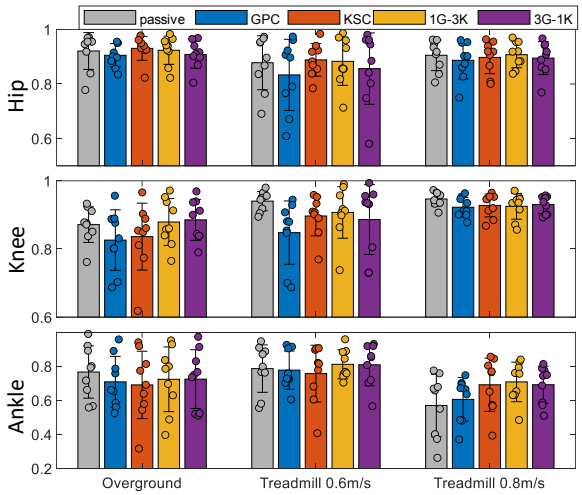

Figure 6. Correlation to natural walking joint trajectories computed during overground and treadmill walking for the (A) hip, (B) knee, and (C) ankle.

The 1G-3K has the closest average step time to both overground and treadmill natural walking at 0.8 m/s. However, at 0.6m/s on the treadmill, GPC demonstrates the most natural step time on average. For overground walking, the average step length is most similar to natural walking with 3G-1K and closely followed by 1G-3K and KSC. Treadmill walking at 0.6 and 0.8m/s results in a more natural step length with KSC and GPC, respectively ($p<0.0039$).

These spatiotemporal metrics demonstrate the effectiveness of the controllers in producing some aspects of natural gait. Among the tested controllers, 1G-3K had the best spatiotemporal performance. An in-depth analysis of the joint-level effects of controllers will reveal whether the resulting gait resembles natural walking.

C. Joint kinematics

Fig.6 shows the average Pearson correlation of each joint angle between natural walking and each test condition.

The average correlation coefficients at the hip joint are high for all conditions and controllers ($R\geq 0.8 \pm 0.04$). During overground and treadmill walking at 0.6m/s, KSC exhibits the highest correlation ($R= 0.93\pm0.04$ and 0.89 ± 0.06, respectively) to natural walking at the hip. Meanwhile, 1G-3K has the highest correlation during 0.8m/s treadmill walking ($R= 0.90\pm0.06$). In treadmill walking at 0.6m/s, a significant difference is observed between passive and GPC performance at the hip ($p=0.002$, significance level adjusted to 0.05/10 with Bonferroni correction). No other significant differences observed between conditions for other joints ($p>0.0059$).

The average correlations at the knee joint range between 0.8 and 0.95. During treadmill walking, the passive conditions have the highest correlation to natural walking at the knee joint. The second highest correlations for treadmill walking at 0.6 and 0.8m/s are during 1G-3K and 3G-1K, respectively. Meanwhile, during overground walking, 3G-1K has the highest knee correlation. The ankle joint has the lowest correlations ranging between 0.5 and 0.8. The highest correlation at the ankle joint occurs during 1G-3K and passive walking for treadmill and overground walking, respectively.

Fig. 7 shows each joint's average ROM during the exoskeleton walking conditions as a percent change from the ROM of natural walking. These obtained results comply with findings of similar studies analyzing the effects of load on gait kinematics showing that walking with the exoskeleton tends to increase hip and ankle ROM, while decreasing the knee ROM compared to no-load walking [27], [28].

The hip ROM is, on average, 20% larger ($\sim8°$) compared to natural walking. During overground and treadmill walking, passive exoskeleton walking has the most natural hip ROM. On average, the knee ROM decreases by 15% ($\sim9°$) compared to natural walking. At the knee joint during overground walking and treadmill walking at 0.8m/s, the most natural ROM occurs during 3G-1K, meanwhile, the most natural range occurs during GPC for treadmill walking at 0.6m/s. However, there are no significant differences between any of the conditions or controllers for the knee or hip ($p>0.0098$).

The ankle joint shows little change in ROM during overground walking and an average increase of close to 30% ($\sim7°$) during treadmill walking. The 1G-3K has, on average, the most natural ankle ROM during overground walking, and the second most natural range during treadmill walking.

This analysis demonstrates that 1G-3K, among the tested active controllers, is preferable at both the knee and hip joints. Align with the spatiotemporal analysis, this suggests that 1G-3K produces a closer to natural gait. As the tested controllers do not directly control joint positions, any observed differences in joint trajectories provide insight into how the exoskeleton is assisting or restricting movements.

D. Muscle activation

The overall effort is computed by summing individual muscular efforts shown in Fig.8 as the percent change from the passive exoskeleton walking effort. On average, KSC, 3G-1K, and 1G-3K result in decreased overall muscle effort for both treadmill and overground walking compared to passive exoskeleton walking. The average decreases range from 5% to 25% and are statistically significant ($p<0.0039$) for all cases except for KSC during treadmill walking at 0.6m/s.

IEEE Robotics and Automation Letters (RA-L) paper, presented at ICRA 2024, Yokohama, Japan. Cite as RA-L paper.

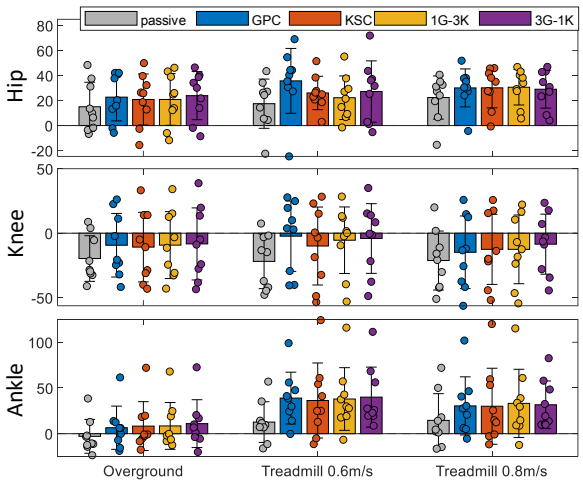

Figure 7. Range of motion during overground and treadmill walking for the (A) hip, (B) knee, and (C) ankle. The ranges are reported in terms of percent change from the natural walking range for each participant.

The hip flexors and knee extensors, RF and VM, have decreases in muscle effort with both 1G-3K and 3G-1K for all walking conditions compared to passive walking. These decreases range from 10 to 55% and are statistically significant for the VM only with 1G-3K (p=0.004). In KSC, muscle effort decreases during treadmill walking at 0.8m/s and overground walking but increases in treadmill walking at 0.6m/s. Conversely, GPC shows a slight increase in effort, in all conditions, suggesting that 1G-3K and 3G-1K controllers are most effective at assisting hip flexion and knee extension.

The knee flexor muscle effort, BF, increased by 5% on average for all controllers during overground and treadmill walking at 0.8m/s. In 0.6 m/s treadmill walking, in contrast, it decreases slightly with all controllers except GPC. However, these changes are not statistically significant ($p>0.049$). The increase in activation of the BF muscle is likely due to the co-contraction required to modulate joint stiffness.

The TA muscle effort increases during all conditions with the exception of 3G-1K during overground and GPC during 0.6m/s treadmill walking. The decreases in these two cases are relatively small (<8%). The TA's primary role is to dorsiflex the ankle during the late swing and stabilize the ankle (co-contracting with plantar flexors [34]) during the stance. As the exoskeleton does not affect the ankle joint during the swing phase, the increase in activation during treadmill walking can be attributed to a perceived need for more stabilization and toe clearance in order to coordinate walking with the exoskeleton controllers.

The GM and SO muscles are ankle plantar flexors, while GM contributes to knee flexion. These muscles effort have decreased between 2 and 24% with all controllers during treadmill and overground walking. The decrease in the effort is statistically significant for 1G-3K ($p<0.0098$) during overground and treadmill walking at 0.8m/s, and 3G-1K during treadmill walking at 0.8m/s (p=0.0098). As the ankle joint is not directly controlled by the exoskeleton, the decrease in activation in ankle plantar flexors demonstrates that the ankle is not required to exert as much power to attain the same walking speed as a result of the provided assistance at

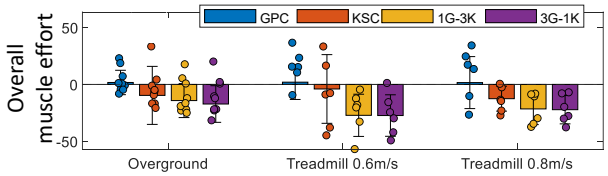

Figure 8. Overall muscular effort percent change from passive exoskeleton walking, computed as the sum of all individual muscle efforts, during the whole gait cycle.

the knee and hip joints. A decrease in GM activation suggests that the exoskeleton is able to assist with knee flexion.

Although many muscles exhibit reduced activation and effort compared to passive exoskeleton walking, these changes are not statistically significant. On average, the 1G-3K and 3G-1K excel in decreasing muscular effort. Notably, during overground walking, this reduction is more pronounced, given the higher average walking speed at these conditions, which would typically elevate the effort. This demonstrates these controllers' ability to further decrease overground walking effort if the speed remained constant for all trials.

E. Muscle co-contraction

The average co-contraction of each muscle pair is shown in Fig. 9. The muscle pairs in the thigh segment are the RF-BF and VM-BF. The RF-BF pair shows a decrease in co-contraction during all conditions with 1G-3K as well as with KSC and 3G-1K during treadmill walking. During treadmill walking at 0.8m/s, there is a large increase in VM-BF co-contraction with KSC. This behavior is exhibited in only six of the participants while the remaining participants exhibit a negligible increase. The large standard deviation of this co-contraction could be an indicator of measurement inaccuracies or due to different strategies adopted by different subjects when interacting with the exoskeleton. The RF-BF pair is responsible for hip and knee stabilization by modulating joint impedance [35] while the VM-BF pair is only involved in knee stiffness modulation and stabilization [36]. The decreases in both muscle pairs during overground walking with KSC, 1G-3K, and 3G-1K indicate that the controller does not induce instability at these joints which could be due to the synchronization of applied torques and intended movements. As the 1G-3K is able to decrease co-activation in both pairs during treadmill walking and in RF-BF during treadmill walking, this controller is best able to provide stability to the participant. The TA-GM and TA-SO are the muscle pairs that dominantly modulate ankle mechanical stiffness. There is a slight decrease in TA-GM co-contraction during treadmill walking at 0.6m/s with GPC and KSC while the rest of the controllers and walking conditions show an increase in co-contraction. TA-SO pair exhibits a decrease in co-contraction with all controllers during treadmill walking at 0.6m/s. The TA-GM and TA-SO muscle pairs are involved in ankle stiffness modulation and stabilization. Higher co-contraction of these pairs during overground walking is due to the increased walking speed compared to passive exoskeleton walking [37]. In contrast, decreased co-contractions during treadmill walking suggests

IEEE Robotics and Automation Letters (RA-L) paper, presented at ICRA 2024, Yokohama, Japan. Cite as RA-L paper.

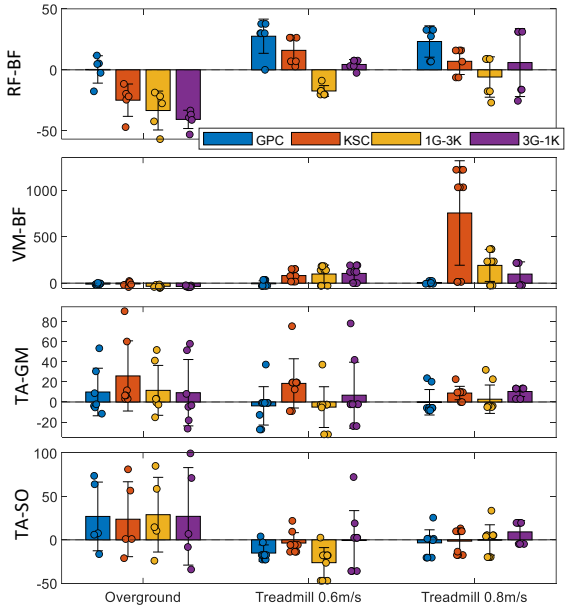

Figure 9. Average integrated co-contraction for each active controller percent change from passive exoskeleton walking.

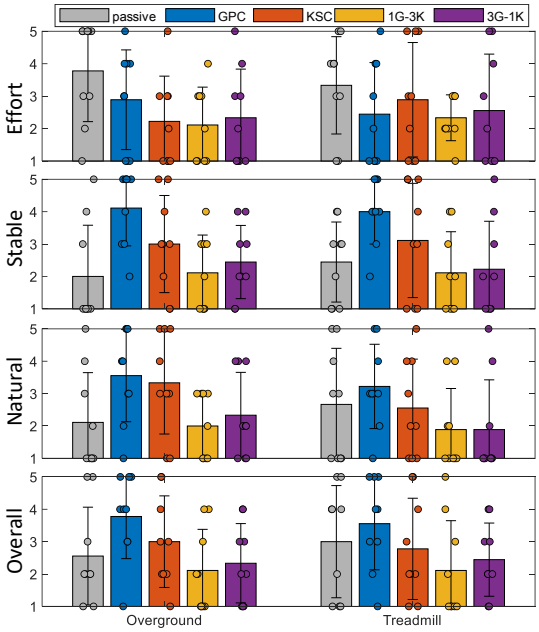

Figure 10. Average participant feedback on effort level, natural walking, stability, and overall performance for treadmill and overground walking with each exoskeleton condition where 1 is the best and 5 is the worst. Each point shows the rating of each participant.

that the user does need to further stabilize the ankle during constant-speed treadmill walking.

On average, the co-contraction is lowest with the 1G-3K controller indicating less joint stiffness and need for further stabilization from the participants is required. This complies with the user response not to conservatively stabilize the joints with co-contraction. The decreases with GPC and 1G-3K compared to passive are statistically significant in the TA-SO muscle pair during treadmill walking ($p<0.006$). The co-contraction decrease compared to passive exoskeleton walking for 1G-3K and 3G-1K is statistically significant in the VM-BF muscle pair during overground walking ($p<0.004$). There are no other significant differences between conditions for other muscle pairs or walking conditions ($p>0.015$).

F. Participant feedback

Fig. 10 shows the average ranking of each exoskeleton condition on effort, natural feel, stability, and overall performance. A ranking of 1 is best, while 5 is worst. On average, passive exoskeleton walking required the highest effort. Active controllers showed similar effort ratings. Compared to the EMG recordings in the previous subsection, the active controls reduced the activation of RF, GM, and SO but increased BF, VM, and TA activation. Unmeasured muscles may also have affected the perceived effort.

The GPC and KSC are rated on average the least natural. This aligns with the kinematic and spatiotemporal analyses in sections III-C and III-B. During overground walking, 1G-3K and passive walking are rated the best, on average. Notably, 1G-3K has the most natural step time, percent stance, and step length in terms of both magnitude and variation. Passive walking exhibits less natural spatiotemporal measures, however, its joint angles and ROM show the highest correlations with natural walking. During treadmill walking, 1G-3K and 3G-1K are rated the most natural in terms of walking speed.

The stability of the GPC is rated the lowest while 1G-3K has the best rating, which complies with the reported co-contractions in Fig. 9. KSC does not restrict user movements, however, it can become unstable due to solely relying on the current measured kinematics. GPC offers stability and predictability, however, can lead to restrictive torques or user-asynchrony. Combining both controllers integrates synchrony from the KSC and stability from GPC. However, the users perceived low stability for the GPC, potentially due to subjective interpretation of stability (which is one of the limitations of using such questionnaires) and user-controller asynchrony, which can be perceived as instability. Overall, 1G-3K has the most favorable rating across all metrics including the overall rating (Fig.10). Although subjective interpretations influence questionnaire results, they support findings from kinematic, spatiotemporal, and EMG signal analyses.

IV. Conclusion

A kinematic state-based torque controller (KSC) and a gait phase-dependent torque controller (GPC) were linearly combined to provide joint torques in a lower limb exoskeleton. Nine participants tested four controllers, ranging from pure KSC to pure GPC for overground and treadmill walking at various speeds. The linear combination of the two controllers, with more weight on KSC, enabled faster walking, closer to natural gait in spatiotemporal measures, and reduced overall muscle activation compared to passive exoskeleton walking. Thigh muscle co-contraction decreased during overground walking with all controllers. In treadmill walking, only the linearly combined controllers reduced co-contraction in thigh and shank muscles and were preferred by most users for their stability, comfort, and natural feel compared to other

IEEE Robotics and Automation Letters (RA-L) paper, presented at ICRA 2024, Yokohama, Japan. Cite as RA-L paper.

controllers. This controller can be augmented with a feedback controller such as a path controller in the future.

The proposed controllers can be applied to overground walking, benefiting from the independence of GPC and KSC from force plate or instrumented insoles. The torque lookup table used in GPC, though not fully personalized, offers potential for improvement through methods like predictive musculoskeletal simulators [38] or neuromechanical models [7]. Future work may involve optimizing the combination weight for diverse populations with mobility impairments.

REFERENCES

[1] L. Mertz, "The next generation of exoskeletons: lighter, cheaper devices are in the works," IEEE pulse, vol. 3, no. 4, pp. 56–61, 2012.

[2] R. Baud, A. R. Manzoori, A. Ijspeert, and M. Bouri, "Review of control strategies for lower-limb exoskeletons to assist gait," Journal of NeuroEngineering and Rehabilitation, vol. 18, no. 1, 2021.

[3] A. Duschau-Wicke, J. Von Zitzewitz, A. Caprez, L. Lunenburger, and R. Riener, "Path control: a method for patient-cooperative robot-aided gait rehabilitation," IEEE Transactions on Neural Systems and Rehabilitation Engineering, vol. 18, no. 1, pp. 38–48, 2009.

[4] A. Martinez, B. Lawson, C. Durrough, and M. Goldfarb, "A velocity-field-based controller for assisting leg movement during walking with a bilateral hip and knee lower limb exoskeleton," IEEE Transactions on Robotics, vol. 35, no. 2, pp. 307–316, 2018.

[5] R. Nasiri, M. Shushtari, H. Rouhani, and A. Arami, "Virtual energy regulator: A time-independent solution for control of lower limb exoskeletons," IEEE Robotics and Automation Letters, vol. 6, no. 4, pp. 7699–7705, 2021.

[6] M. Shushtari, R. Nasiri, and A. Arami, "Online reference trajectory adaptation: A personalized control strategy for lower limb exoskeletons," IEEE Robotics and Automation Letters, vol. 7, no. 1, pp. 128–134, 2021.

[7] G. Durandau, W. F. Rampeltshammer, H. van der Kooij, and M. Sartori, "Neuromechanical model-based adaptive control of bilateral ankle exoskeletons: biological joint torque and electromyogram reduction across walking conditions," IEEE Transactions on Robotics, vol. 38, no. 3, pp. 1380–1394, 2022.

[8] Sado, Fatai and Yap, Hwa Jen and Ghazilla, Raja Ariffin Raja and Ahmad, Norhafizan, "Exoskeleton robot control for synchronous walking assistance in repetitive manual handling works based on dual unscented kalman filter," PloS one, vol. 13, no. 7, p. e0200193, 2018.

[9] W. van Dijk, H. van der Kooij, B. Koopman, E. H. F. van Asseldonk, and H. van der Kooij, "Improving the transparency of a rehabilitation robot by exploiting the cyclic behaviour of walking," in 2013 IEEE 13th International Conference on Rehabilitation Robotics (ICORR), 2013, pp. 1–8.

[10] T. Nakamura, K. Saito, and K. Kosuge, "Control of wearable walking support system based on human-model and grf," in Proceedings of the 2005 IEEE international conference on robotics and automation. IEEE, 2005, pp. 4394–4399.

[11] M. Li, J. Deng, F. Zha, S. Qiu, X. Wang, and F. Chen, "Towards online estimation of human joint muscular torque with a lower limb exoskeleton robot," Applied Sciences (Switzerland), vol. 8, no. 9, 2018.

[12] F. Just, Ö. Özen, S. Tortora, R. Riener, and G. Rauter, "Feedforward model based arm weight compensation with the rehabilitation robot armin," in 2017 International Conference on Rehabilitation Robotics (ICORR). IEEE, 2017, pp. 72–77.

[13] G. M. Bryan, P. W. Franks, S. Song, A. S. Voloshina, R. Reyes, M. P. O'Donovan, K. N. Gregorczyk, and S. H. Collins, "Optimized hip–knee–ankle exoskeleton assistance at a range of walking speeds," Journal of neuroengineering and rehabilitation, vol. 18, no. 1, pp. 1–12, 2021.

[14] A. Gams, T. Petrič, T. Debevec, and J. Babič, "Effects of robotic knee exoskeleton on human energy expenditure," IEEE Transactions on Biomedical Engineering, vol. 60, no. 6, pp. 1636–1644, 2013.

[15] S. Yu, T.-H. Huang, D. Wang, B. Lynn, D. Sayd, V. Silivanov, Y. S. Park, Y. Tian, and H. Su, "Design and control of a high-torque and highly backdrivable hybrid soft exoskeleton for knee injury prevention during squatting," IEEE Robotics and Automation Letters, vol. 4, no. 4, pp. 4579–4586, 2019.

[16] M. Jeong, H. Woo, and K. Kong, "A study on weight support and balance control method for assisting squat movement with a wearable robot, angel-suit," International Journal of Control, Automation and Systems, vol. 18, no. 1, pp. 114–123, 2020.

[17] J. Zhang, P. Fiers, K. A. Witte, R. W. Jackson, K. L. Poggensee, C. G. Atkeson, and S. H. Collins, "Human-in-the-loop optimization of exoskeleton assistance during walking," Science, vol. 356, no. 6344, pp. 1280–1284, 2017.

[18] R. D. Gregg, T. W. Bretl, and M. W. Spong, "A control theoretic approach to robot-assisted locomotor therapy," in 49th IEEE Conference on Decision and Control (CDC), 2010, pp. 1679–1686.

[19] J. Bae, K. Kong, and M. Tomizuka, "Real-time estimation of lower extremity joint torques in normal gait," IFAC Proceedings Volumes, vol. 42, no. 16, pp. 443–448, 2009.

[20] H. Dinovitzer, M. Shushtari, and A. Arami, "Accurate real-time joint torque estimation for dynamic prediction of human locomotion," IEEE Transactions on Biomedical Engineering, vol. 70, no. 8, pp. 2289–2297, 2023.

[21] M. Shushtari, H. Dinovitzer, J. Weng, and A. Arami, "Ultra-robust real-time estimation of gait phase," IEEE Transactions on Neural Systems and Rehabilitation Engineering, vol. 30, pp. 2793–2801, 2022.

[22] D. A. Winter and D. Robertson, "Joit torque and energy patterns in normal gait," Biological cybernetics, vol. 29, no. 3, pp. 137–142, 1978.

[23] H. Yu and B. M. Wilamowski, "Levenberg-marquardt training," Industrial electronics handbook, vol. 5, no. 12, p. 1, 2011.

[24] J. Rueterbories, E. G. Spaich, B. Larsen, and O. K. Andersen, "Methods for gait event detection and analysis in ambulatory systems," Medical engineering & physics, vol. 32, no. 6, pp. 545–552, 2010.

[25] T. McGrath, R. Fineman, and L. Stirling, "An auto-calibrating knee flexion-extension axis estimator using principal component analysis with inertial sensors," Sensors, vol. 18, no. 6, p. 1882, 2018.

[26] A. Arami, N. L. Tagliamonte, F. Tamburella, H.-Y. Huang, M. Molinari, and E. Burdet, "A simple tool to measure spasticity in spinal cord injury subjects," in 2017 International Conference on Rehabilitation Robotics (ICORR). IEEE, 2017, pp. 1590–1596.

[27] D. Majumdar, M. S. Pal, and D. Majumdar, "Effects of military load carriage on kinematics of gait," Ergonomics, vol. 53, no. 6, pp. 782–791, 2010.

[28] X. Qu and J. C. Yeo, "Effects of load carriage and fatigue on gait characteristics," Journal of biomechanics, vol. 44, no. 7, pp. 1259–1263, 2011.

[29] B. Mariani, S. Rochat, C. J. Büla, and K. Aminian, "Heel and toe clearance estimation for gait analysis using wireless inertial sensors," IEEE Transactions on Biomedical Engineering, vol. 59, no. 11, pp. 3162–3168, 2012.

[30] R. D. Crowninshield and R. A. Brand, "A physiologically based criterion of muscle force prediction in locomotion," Journal of biomechanics, vol. 14, no. 11, pp. 793–801, 1981.

[31] M. Shushtari, A. Takagi, J. Lee, E. Burdet, and A. Arami, "Balance strategy in hoverboard control," Scientific reports, vol. 12, no. 1, pp. 1–11, 2022.

[32] McDonald, JH, "Handbook of biological statistics: Multiple comparisons," Handbook of Biological Statistics, pp. 256–259, 2008.

[33] L. Hak, H. Houdijk, P. J. Beek, and J. H. van Dieën, "Steps to take to enhance gait stability: the effect of stride frequency, stride length, and walking speed on local dynamic stability and margins of stability," PloS one, vol. 8, no. 12, p. e82842, 2013.

[34] H. Lee, E. J. Rouse, and H. I. Krebs, "Summary of human ankle mechanical impedance during walking," IEEE journal of translational engineering in health and medicine, vol. 4, pp. 1–7, 2016.

[35] H. Y. Huang, A. Arami, I. Farkhatdinov, D. Formica, and E. Burdet, "The influence of posture, applied force and perturbation direction on hip joint viscoelasticity," IEEE Transactions on Neural Systems and Rehabilitation Engineering, vol. 28, no. 5, pp. 1138–1145, 2020.

[36] S. Pfeifer, H. Vallery, M. Hardegger, R. Riener, and E. J. Perreault, "Model-based estimation of knee stiffness," IEEE transactions on biomedical engineering, vol. 59, no. 9, pp. 2604–2612, 2012.

[37] D. S. Peterson and P. E. Martin, "Effects of age and walking speed on coactivation and cost of walking in healthy adults," Gait & posture, vol. 31, no. 3, pp. 355–359, 2010.

[38] J. Weng, E. Hashemi, and A. Arami, "Natural Walking With Musculoskeletal Models Using Deep Reinforcement Learning," IEEE Robotics and Automation Letters, vol. 6, no. 2, pp. 4156–4162, 2021.

IEEE Robotics and Automation Letters (RA-L) paper, presented at ICRA 2024, Yokohama, Japan. Cite as RA-L paper.